RESEARCH ARTICLE

genesis The Journal of Genetics and Development WILEY

Increased activity of mesenchymal ALK2-BMP signaling causes posteriorly truncated microglossia and disorganization of lingual tissues

Mohamed Ishan[1] | Guiqian Chen[1] | Chenming Sun[2] | Shi-You Chen[2] | Yoshihiro Komatsu[3] | Yuji Mishina[4] | Hong-Xiang Liu[1]

[1]Department of Animal and Dairy Science, Regenerative Bioscience Center, College of Agricultural and Environmental Sciences, University of Georgia, Athens, Georgia

[2]Department of Physiology and Pharmacology, College of Veterinary Medicine, University of Georgia, Athens, Georgia

[3]Department of Pediatrics, The University of Texas Medical School at Houston, Houston, Texas

[4]Department of Biologic and Materials Sciences, School of Dentistry, University of Michigan, Ann Arbor, Michigan

Correspondence
Hong-Xiang Liu, Department of Animal and Dairy Science, Regenerative Bioscience Center, College of Agricultural and Environmental Sciences, University of Georgia, Athens, GA 30602.
Email: lhx@uga.edu

Present address: Guiqian Chen, Zhejiang Provincial Key Laboratory of Silkworm Bioreactor and Biomedicine and College of Life Sciences and Medicine, Zhejiang Sci-Tech University, Hangzhou 310018, China.

Summary

Proper development of taste organs including the tongue and taste papillae requires interactions with the underlying mesenchyme through multiple molecular signaling pathways. The effects of bone morphogenetic proteins (BMPs) and antagonists are profound, however, the tissue-specific roles of distinct receptors are largely unknown. Here, we report that constitutive activation (ca) of ALK2-BMP signaling in the tongue mesenchyme (marked by *Wnt1-Cre*) caused microglossia—a dramatically smaller and misshapen tongue with a progressively severe reduction in size along the anteroposterior axis and absence of a pharyngeal region. At E10.5, the tongue primordia (branchial arches 1–4) formed in *Wnt1-Cre/caAlk2* mutants while each branchial arch responded to elevated BMP signaling distinctly in gene expression of BMP targets (*Id1*, *Snai1*, *Snai2*, and *Runx2*), proliferation (*Cyclin-D1*) and apoptosis (*p53*). Moreover, elevated ALK2-BMP signaling in the mesenchyme resulted in apparent defects of lingual epithelium, muscles, and nerves. In *Wnt1-Cre/caAlk2* mutants, a circumvallate papilla was missing and further development of formed fungiform papillae was arrested in late embryos. Our data collectively demonstrate that ALK2-BMP signaling in the mesenchyme plays essential roles in orchestrating various tissues for proper development of the tongue and its appendages in a region-specific manner.

KEYWORDS
apoptosis, bone morphogenetic protein signaling, branchial arch, microglossia, proliferation, tongue mesenchyme

1 | INTRODUCTION

The mammalian tongue is an organ comprised of multiple highly organized tissues that enable its critical functions, including speaking, food processing, and taste sensation. Developmental defects in the tongue such as aglossia, macroglossia, microglossia, and ankyloglossia (Chandrashekar, Kashinath, & Suhas, 2014) can cause serious disease conditions like dysphasia, dysphagia, and dysgeusia. The development of the tongue requires tissue–tissue interactions governed by multiple signaling pathways (Iwata, Suzuki, Pelikan, Ho, & Chai, 2013; Liu et al., 2009; Liu, Grosse, et al., 2012; Liu, Komatsu, Mishina, & Mistretta, 2012; Liu, MacCallum, Edwards, Gaffield, & Mistretta, 2004; Millington et al., 2017). Thus, studies on the organogenesis and molecular regulation of the tongue and its appendages will help to understand the mechanisms underlying the tongue anomalies.

In mice, emergence of the tongue starts with the appearance of three lingual swellings from the first branchial arch (BA 1) at gestational day (E) 11.5. These swellings fuse and form the anterior two thirds of

the tongue—the oral tongue at E12.5. Concurrently with the formation of the oral tongue, a small midline swelling (the copula) develops from BA 2 and fuses with another midline swelling originating from BAs 3–4 to form the posterior third of the tongue—the pharyngeal tongue (Cobourne et al., 2018). At this stage, myoblast cells migrate into the developing tongue and differentiate to become intrinsic glossal muscles (Cobourne et al., 2018; Millington et al., 2017). Meanwhile, taste papilla placodes emerge on the dorsal surface (Mbiene, Maccallum, & Mistretta, 1997; Mistretta, 1972) and will develop into taste papillae that host taste buds. The proper formation of the tongue and its appendages is an integrated process that requires a tight coordination among BAs 1–4 and various types of tissues/cells.

Bone morphogenetic proteins (BMP) are secreted proteins that may act in a paracrine manner to activate intracellular signaling in the surrounding cells and play crucial roles in cell growth, differentiation, and apoptosis during the development of many organs (Bragdon et al., 2011; Wang et al., 2014). BMPs bind to the Type II BMP receptors (BMPR2, ACVRII), activate Type I BMP receptors (ALK2, ALK3, and ALK6) and phosphorylate downstream signaling component Smad1, 5, and 8 to promote the expression of BMP target genes (e.g., *Id1*, *Snai1*, *Snai2*, and *Runx2*). Type I BMP receptors are known to be the main determinants of the downstream signaling activity (Wang et al., 2014). It has been reported that BMP ligands (BMP 2, 3, 4, 6, and 7), antagonists (noggin and follistatin) and receptors (ALK2, ALK3, and ALK6) are present in both epithelium and mesenchyme of the developing tongue (Beites et al., 2009; Jung, Oropeza, & Thesleff, 1999; Kawasaki et al., 2012; Suga et al., 2007; Zhou, Liu, & Mistretta, 2006). The effects of BMP ligands and their antagonists in the tongue and taste papilla development are profound (Beites et al., 2009; Zhou et al., 2006). However, the specific roles of mediating receptors and involved tissue compartments of BMP signaling in tongue organogenesis are largely unknown.

Constitutive activation of *ALK3* in the neural crest and derived mesenchyme causes a slightly defected tongue in a previous study focusing on cleft palate formation and delayed tooth differentiation (Li et al., 2013). In the present study, we report that a proper level of ALK2-mediated BMP (hereafter ALK2-BMP) signaling in neural crest and derived mesenchymal cells (marked by *Wnt1-Cre*) is essential in regulating proliferation and apoptosis of these cells at an early embryonic stage for the proper tongue shape and size. Also, ALK2-BMP signaling plays important regulatory roles in mesenchymal interactions with other lingual tissues for their organization, and the development of taste papillae and taste buds.

2 | RESULTS

2.1 | Constitutive activation of ALK2-BMP signaling in neural crest and derived mesenchymal cells results in posteriorly truncated microglossia

To elevate the activity of type I BMP receptor ALK2-mediated BMP (hereafter ALK2-BMP) signaling in the tongue mesenchyme, transgenic mouse model with a constitutively activated (ca) form of *Alk2* (*caAlk2*) (Fukuda et al., 2006) was used to cross with *Wnt1-Cre* that mark neural

crest-derived mesenchymal cells in the tongue (Liu, Komatsu, et al., 2012; Thirumangalathu, Harlow, Driskell, Krimm, & Barlow, 2009). Compared to *Cre⁻/caAlk2* littermate controls (Figure 1a), deficiencies were evident in multiple craniofacial regions of E12.5 *Wnt1-Cre/caAlk2* mouse embryos including brain (Figure 1b, arrow), eyes (Figure 1b, arrowhead), and orofacial region (Figure 1b, open arrowhead). Mutant mice had microglossia (Figure 1d,f), with a significantly smaller tongue in mutants than that in littermate controls (526.51 ± 14.18 μm vs. 1,163.09 ± 13.78 μm in length of oral tongue, $p < .01$ in Figure 1g; 352.43 ± 6.5 μm vs. 749.23 ± 4.25 μm in width, $p < .01$ in Figure 1h). In the majority of *Wnt1-Cre/caAlk2* mouse embryos, tongue swellings fused at the midline for a unitary tongue tip (24 mutants out of 32, Figure 1d,f) while some had a bifid anterior tongue (8 mutants out of 32, image not shown). A progressive decrease in tongue size was consistently observed along the anteroposterior axis in all of the mutants (tongues with a unitary or bifid tip). Although the *Wnt1-Cre/caAlk2* mutant tongue was smaller, fungiform taste papilla placodes were observed on the anterior tongue region (Figure 1d,f, arrowheads) similarly to those in the littermate control (Figure 1c,e, arrowheads). On the smaller anterior tongues, fewer rows of fungiform taste papillae were seen and there was not an apparent change of density of papilla placodes. In the position where a distinct circumvallate papilla placode was observed in the littermate control tongues (Figure 1e, arrow), an enlarged Shh⁺ patch of tissue, presumably circumvallate papilla placode, was observed in the tongues of *Wnt1-Cre/caAlk2* mutants (Figure 1f, arrow). A pharyngeal part of the tongue posterior to the presumable Shh⁺ circumvallate was missing in *Wnt1-Cre/caAlk2* mutants (Figure 1f).

2.2 | Fungiform papillae were well developed in the smaller E14.5 *Wnt1-Cre/caAlk2* mutant tongue

At E14.5 when tongue and taste papillae attain their stereotypical shape and spatial distribution (Figure 2a), *Wnt1-Cre/caAlk2* mutants continued to exhibit microglossia (Figure 2b) compared to the *Cre⁻/caAlk2* littermate control (Figure 2a). Developing fungiform taste papillae were observed in the tongue of E14.5 *Wnt1-Cre/caAlk2* mutants (Figure 2b,d, arrowheads, inset in 2d) in similar structure to those of littermate controls (Figure 2a,c, arrowheads, inset in 2c). Similarly to E12.5, there was not an apparent change of papilla density on the smaller anterior tongues. Further, the pharyngeal tongue region was missing and a Shh⁺ circumvallate papilla seen in littermate controls (Figure 2c, arrow) was absent in E14.5 *Wnt1-Cre/caAlk2* mutants (Figure 2d). Similar to E12.5, both unitary (14 out of 18, Figure 2f) and bifid (4 out of 18, Figure 2b,d) anterior tips was observed in the smaller tongues of E14.5 *Wnt1-Cre/caAlk2* mutants.

Next, we examined outgrowth and branching of nerve fibers that traverse through the tongue mesenchyme and innervate the developing taste papillae. At E14.5, in contrast to extensive βIII-tubulin⁺ nerve fibers approaching taste papillae in the littermate control (Figure 2e, open arrowhead), nerve fibers were absent in the vicinity of *Wnt1-Cre/caAlk2* mutant fungiform taste papillae (Figure 2f). Obviously, βIII-tubulin⁺ nerve fibers were present in *Wnt1-Cre/caAlk2* mutant mandible (Figure 2f, open arrowheads). On sections, compared
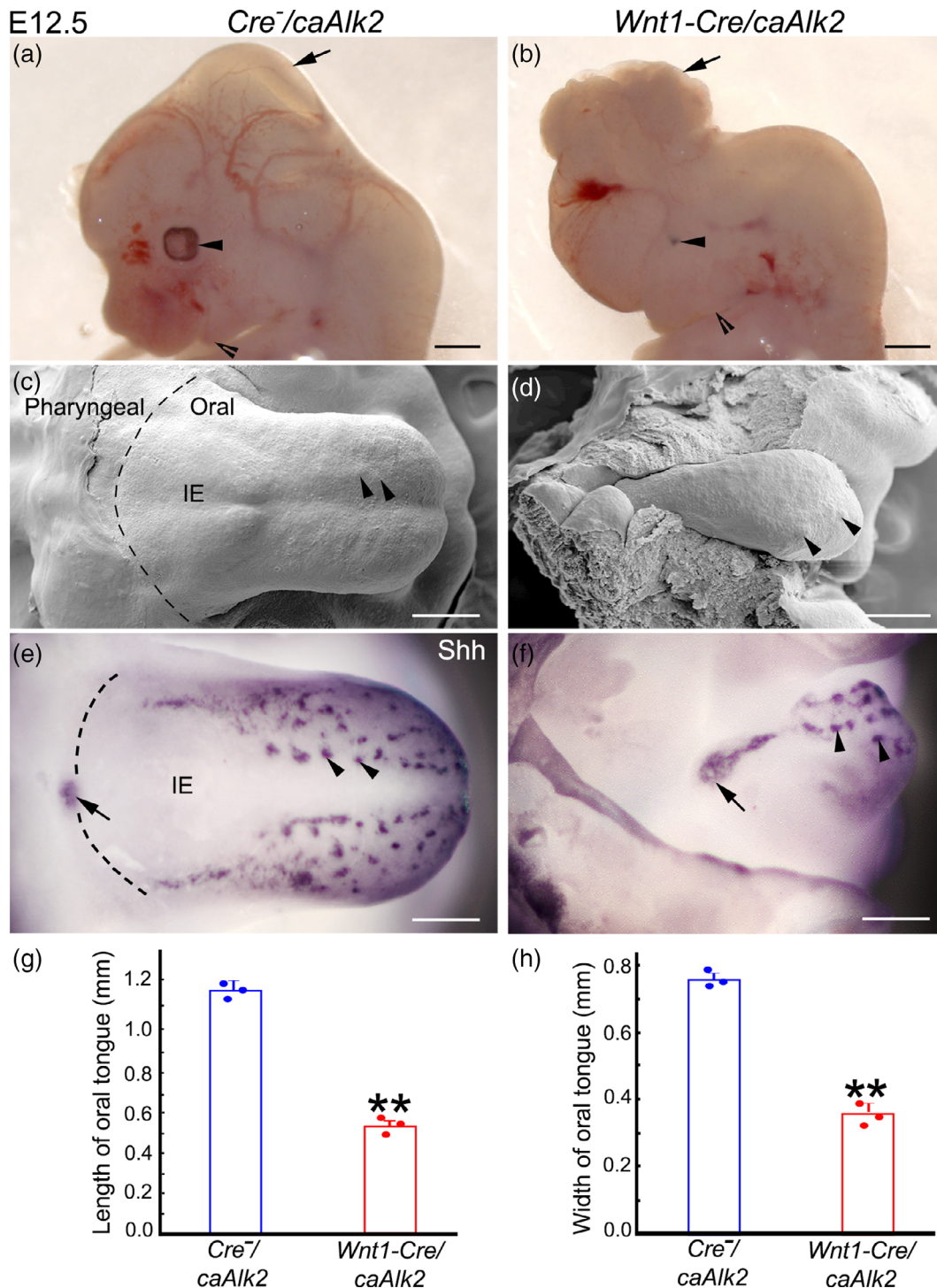
FIGURE 1 Representative images (a–f) and measurement of tongue size (g,h) to illustrate the deficiencies of craniofacial region and tongue in E12.5 *Wnt1-Cre/caAlk2* mutants compared to *Cre⁻/caAlk2* littermate controls. (a, b) Light microscopy images of the heads of a littermate control (a) and *Wnt1-Cre/caAlk2* mutant (b). Arrows point to the brain; arrowheads point to the eye; open arrowheads point to the orofacial region. Scale bars: 1 mm. (c, d) Scanning electron microscopy (SEM) images of littermate control (c) and *Wnt1-Cre/caAlk2* mutant (d) tongues. Scale bars: 200 μm. (e, f) Light microscopy images of whole mount immunoreaction for Shh (blue), a developing taste papilla marker, in littermate control (e) and *Wnt1-Cre/caAlk2* mutant (f) tongues. Arrowheads in c–f point to fungiform taste papilla placodes. The arrow in e and f points to the Shh⁺ circumvallate papilla placode in the posterior oral tongue. Dashed lines in c and e separate the oral tongue from the pharyngeal tongue. IE, intermolar eminence. Scale bars: 200 μm. (g, h) Histograms ($X \pm SD$; $n = 3$) represent the length (g) and width (h) of the oral tongue in *Wnt1-Cre/caAlk2* and littermate controls. **$p \le .01$ Student's *t* test compared to littermate control tongue
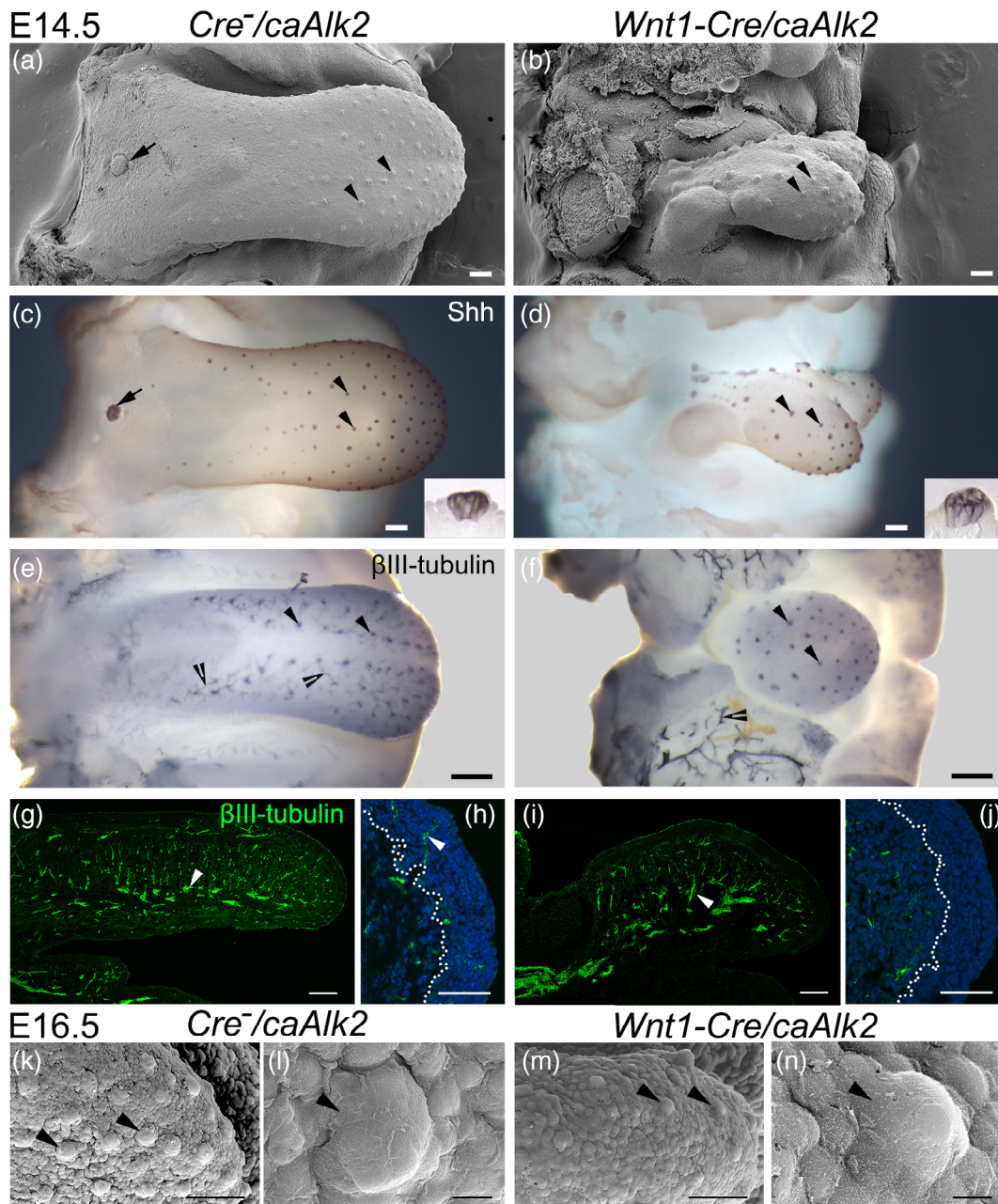
FIGURE 2 Development of tongue and taste papillae in E14.5 and E16.5 *Wnt1-Cre/caAlk2* mutant and *Cre⁻/caAlk2* littermate control mice. (a–f) Whole mount images (scanning electron microscopy in a, b, light microscopy in c–f) of E14.5 littermate control (a, c, e) and *Wnt1-Cre/caAlk2* (b, d, f) tongues. Whole mount immunoreactions were performed against Shh (c, d) or βIII-tubulin (e, f). Insets in c and d show the restriction of Shh immunoproducts to fungiform taste papilla epithelium on tongue sections. Arrowheads in a–f point to developing fungiform taste papillae. Arrows in a and c point to the circumvallate papilla. Open arrowheads in e and f point to βIII-tubulin⁺ nerve fibers in littermate control (e) and *Wnt1-Cre/caAlk2* mutant (f) tongues. Scale bars: 100 μm. (g–j) Single-plane laser scanning confocal images of sagittal sections of littermate control (g) and *Wnt1-Cre/caAlk2* mutant (i) tongues immunostained for βIII-tubulin (green). h and j are high magnification images of the anterior tip of littermate control (h) and *Wnt1-Cre/caAlk2* mutant tongues (j). Arrowheads in g–i point to βIII-tubulin⁺ nerve fibers. Dotted lines in h and j separate the epithelium from the underlying mesenchyme. Scale bars: 100 μm in g, i; 50 μm in h, j. (k–n) SEM images of E16.5 littermate control (k, l) and *Wnt1-Cre/caAlk2* mutant (m, n) tongues to illustrate the left anterior tongue tip (k, m) and a fungiform papilla (l, n) in a littermate control (k, l) and *Wnt1-Cre/caAlk2* mutant (m, n) tongue. Arrowheads point to fungiform papillae. Scale bars: 100 μm in k, m; 10 μm in l, n

to the extensively branched nerve fibers in littermate control tongues (Figure 2g, arrowhead), βIII-tubulin⁺ nerve fibers were loosely distributed in the *Wnt1-Cre/caAlk2* mutant tongue mesenchyme (Figure 2i, arrowhead). Moreover, these fibers did not branch out into taste papillae nor penetrate the epithelium (Figure 2j) in contrast to the

dense distribution of nerve fibers in the papilla core in littermate controls (Figure 2h, arrowhead).

To evaluate the further development of fungiform papillae, E16.5 littermate control (Figure 2k,l) and *Wnt1-Cre/caAlk2* mutant (Figure 2m,n) tongues were examined using scanning electron

microscopy. Similar to E14.5, developing fungiform papillae were observed in the E16.5 *Wnt1-Cre/caAlk2* mutants (Figure 2m,n, arrowheads) similarly in structure to those of littermate controls (Figure 2k,l, arrowheads).

2.3 | Development and organization of multiple lingual tissues were deficient in the E18.5 *Wnt1-Cre/caAlk2* mutant tongue

Wnt1-Cre/caAlk2 mutant mice die shortly after birth, thus E18.5 embryos were harvested as the last stage for phenotypic analyses. Compared to the *Cre⁻/caAlk2* littermate controls (Figure 3a), microglossia in E18.5 *Wnt1-Cre/caAlk2* mutants was evident (Figure 3b). Neither pharyngeal tongue nor circumvallate papilla

(Figure 3a, arrow) was seen in the E18.5 *Wnt1-Cre/caAlk2* mutants (Figure 3b). In the littermate control tongues spine-like filiform papillae (Figure 3a,c,d, open arrowheads) and flaking of the superficial epithelial cells were profound. In contrast, filiform papillae were less profound and epithelial cell flaking was not noticed on the surface of *Wnt1-Cre/caAlk2* mutant tongue (Figure 3b,e,f).

Fungiform papillae were observed in the oral tongue of E18.5 *Wnt1-Cre/caAlk2* mutants (Figure 3b,e,f), however these fungiform papillae (Figure 3e,f, arrowheads) were underdeveloped compared to those of E18.5 littermate controls (Figure 3c,d, arrowheads) as they were similar in appearance to those in E16.5 littermate control (Figure 2k,l, arrowheads) and *Wnt1-Cre/caAlk2* (Figure 2m,n) mutant tongues. Further, early taste buds were detected in the tongue epithelial sheets (Figure 3i, arrowheads) and sagittal tongue sections
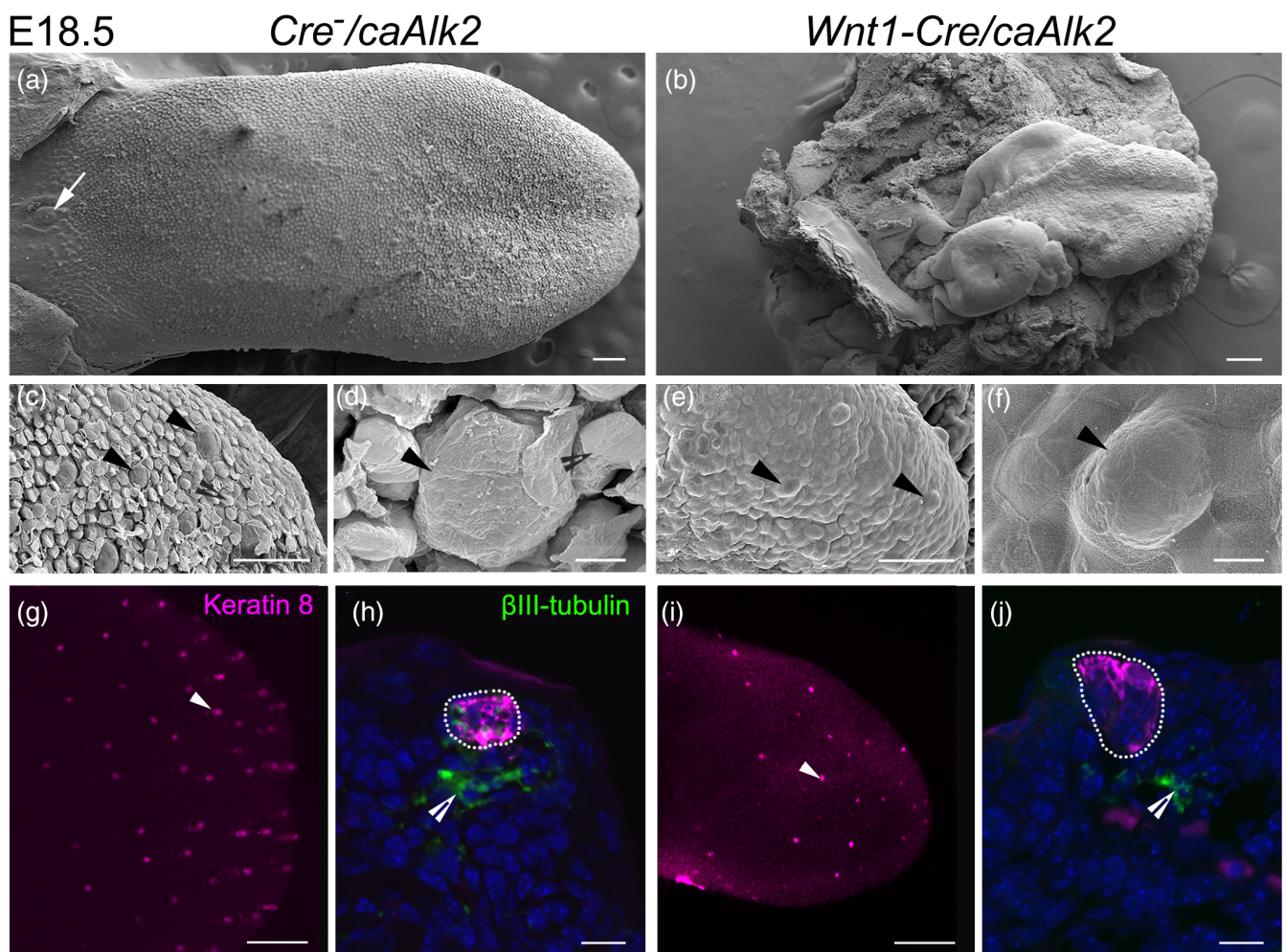

FIGURE 3 Further advancement of taste papilla development and formation of early taste buds in E18.5 *Wnt1-Cre/caAlk2* mutant and *Cre⁻/caAlk2* littermate control tongues. (a–f) SEM images of E18.5 littermate control (a, c, d) and *Wnt1-Cre/caAlk2* mutant (b, e, f) tongues. The arrow in a points to the circumvallate papilla. In c–f, arrowheads point to fungiform papillae, open arrowheads in c, d point to filiform papillae. High-magnification images of the left anterior tongue tip (c, e) and a fungiform papilla (d, f) in a littermate control (a, c, d) and *Wnt1-Cre/caAlk2* mutant (b, e, f) tongue. Scale bars: 500 μm in a, b; 100 μm in c, e; 10 μm in d, f. (g, i) Littermate control (g) and *Wnt1-Cre/caAlk2* mutant (i) tongue epithelial sheets immunostained with pan-taste cell marker K8 (magenta). Arrowheads point to K8⁺ fungiform taste buds. Scale bars: 200 μm. (h, j) Single-plane laser scanning confocal images of sagittal sections of littermate control (h) and *Wnt1-Cre/caAlk2* mutant (j) tongues immunostained with K8 (magenta) and βIII-tubulin (green). Dotted lines in h and j encircle K8⁺ taste buds; open arrowheads point to βIII-tubulin⁺ nerve fibers. Scale bars: 20 μm
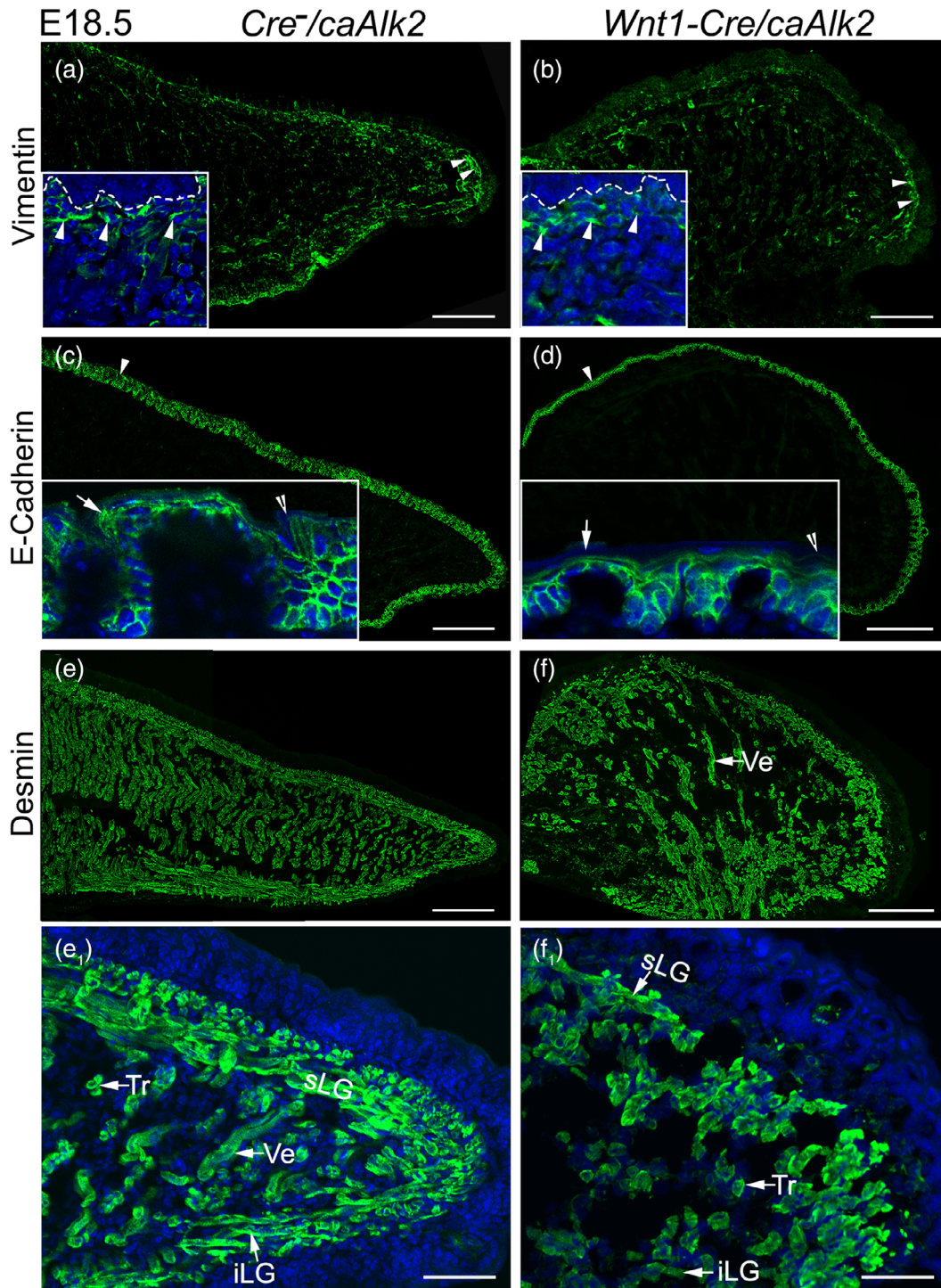
FIGURE 4 Representative photomicrographs of sagittal sections of E18.5 *Wnt1-Cre/caAlk2* mutant and *Cre⁻/caAlk2* littermate control tongues. (a–f) Single-plane laser scanning confocal images of littermate control (a, c, e) and *Wnt1-Cre/caAlk2* mutant (b, d, f) tongues immunostained with mesenchymal cell marker Vimentin (a and b, green), epithelial cell marker E-Cadherin (c and d, green), or muscle cell marker Desmin (e and f, green). Insets in a–d show representative high-magnification images. Arrowheads in a and b point to the dense stromal cell layer under the epithelium. Dashed lines in insets of a and b separate the epithelium from the underlying mesenchyme. Arrows in insets of c and d point to fungiform papillae. Arrowheads in c and d point to the epithelium. Open arrowheads in insets of c and d point to filiform papillae. e_1 and f_1 are high-magnification images of e and f. sLG, superior longitudinal muscle; iLG, inferior longitudinal muscle; Ve, vertical muscle; Tr, transverse muscle. Scale bars: 100 μm in a–f; 50 μm in e_1, f_1

(Figure 3j) of *Wnt1-Cre/caAlk2* mutants with a pan taste cell marker Keratin 8 (K8⁺) as those in littermate control epithelial sheets (Figure 3g, arrowheads) and sagittal sections (Figure 3h). Among the

taste buds detected in the E18.5 *Wnt1-Cre/caAlk2* mutants, 41% had a typical morphology as those in littermate controls (Figure 3h), while the majority (59% as in Figure 3j) appeared to have an increased
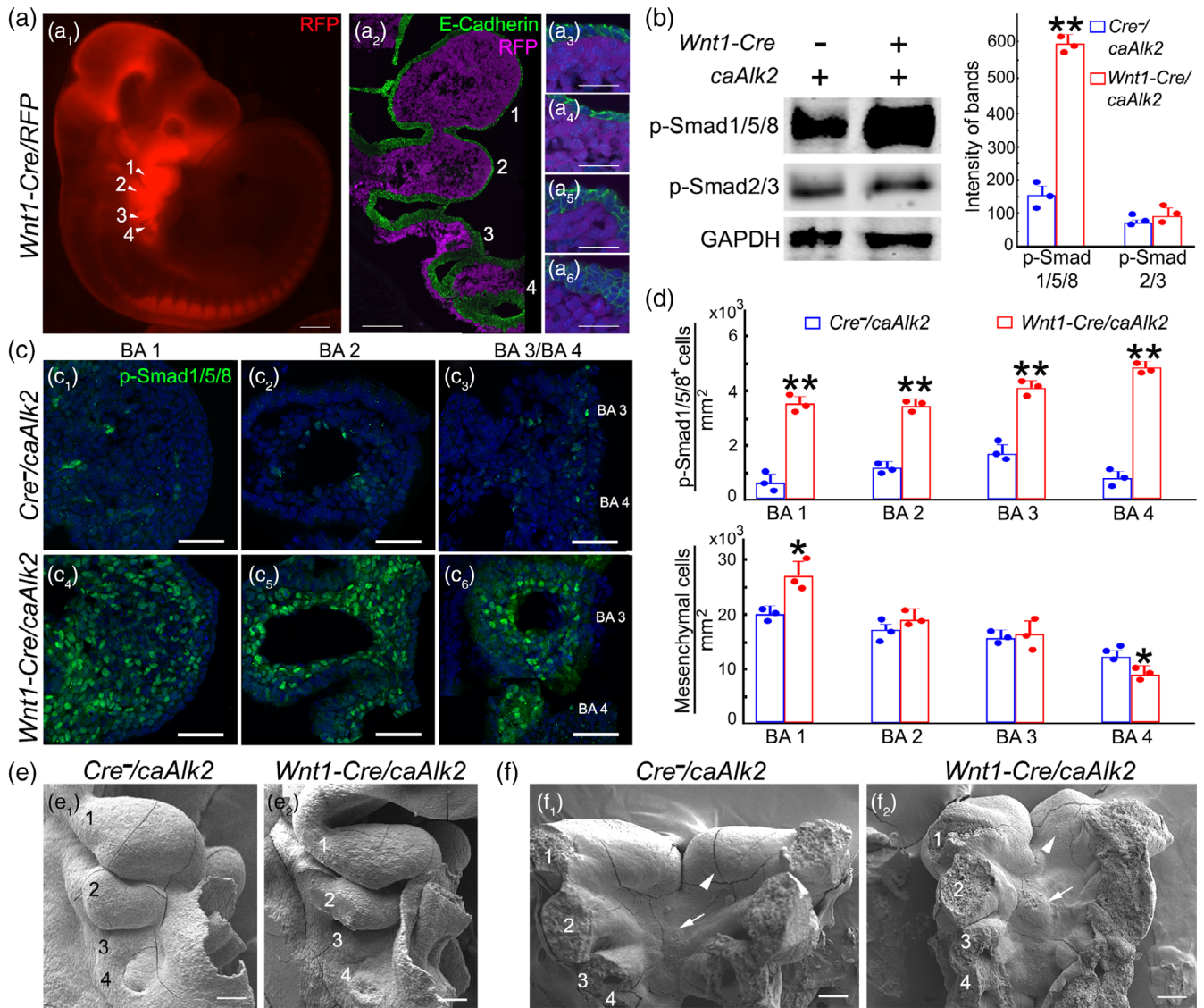
FIGURE 5 Representative photomicrographs of branchial arches (BAs) of E10.5 *Wnt1-Cre/RFP*, *Wnt1-Cre/caAlk2*, and *Cre⁻/caAlk2* littermate controls. (a) Whole mount image of an E10.5 *Wnt1-Cre/RFP* embryo. Numerals 1–4 in a show individual BAs. a_2-a_6 are single-plane laser scanning confocal images of *Wnt1-Cre/RFP* BAs immunostained with E-Cadherin (green). a_3-a_6 are high-magnification images of individual BAs in a_2. Scale bars: 400 μm in a_1; 100 μm in a_2; 50 μm in a_3-a_6. (b) Western blot bands (left) of p-Smad1/5/8, p-Smad2/3, and GAPDH in the mesenchyme of BAs 1–4 of littermate controls and *Wnt1-Cre/caAlk2* mutants. Histogram (right) represents the intensities of Western blot bands of p-Smad1/5/8, p-Smad2/3 as means ± standard deviation ($X \pm SD$; $n = 3$). **$p \leq .01$ Student's t test compared to littermate control group. (c) Single-plane laser scanning confocal images of littermate control (c_1-c_3) and *Wnt1-Cre/caAlk2* (c_4-c_6) BA transverse sections immunostained with p-Smad1/5/8 (green). Scale bars: 50 μm. (d) Histograms ($X \pm SD$; $n = 3$) represent the total number of p-Smad1/5/8⁺ cells per mm² (top) and total number of mesenchymal cells per mm² (bottom) in individual BAs of *Wnt1-Cre/caAlk2* and littermate controls. *$p \leq .05$, **$p \leq .01$ compared to littermate control BAs using two-way ANOVA followed by Fisher's least significant difference (LSD) analyses. (e, f) SEM images to illustrate the side (e) and dorsal (f) view of BAs of a littermate control (e_1, f_1) and *Wnt1-Cre/caAlk2* mutant (e_2, f_2). Numerals 1–4 in e and f mark individual BAs 1–4. Arrowheads in f point to the dorsal swelling of BA 1. Arrows in f point to the copula in BA 2. Scale bars: 100 μm

height from base to apex with most K8⁺ cells located apically. Such shape of taste buds was also observed in E17.5 littermate control and *Wnt1-Cre/caAlk2* tongues (data not shown). In contrast to the dense innervation of taste buds in the littermate controls (Figure 3h, open arrowhead), βIII-tubulin⁺ nerve fibers were absent in taste buds and dramatically reduced in the mesenchymal core of fungiform papillae in *Wnt1-Cre/caAlk2* mutants (Figure 3j, open arrowhead).

Neural crest-derived mesenchyme/connective tissue serves as a scaffold that is important for tissue differentiation and organization (Rinon et al., 2007). To identify the effects of altered ALK2-BMP signaling in the connective tissue, main lingual tissues were examined. Vimentin⁺ stromal cells were extensively distributed in the E18.5 tongue mesenchyme of both littermate controls (Figure 4a) and *Wnt1-Cre/caAlk2* mutants (Figure 4b). A dense layer was obvious in the
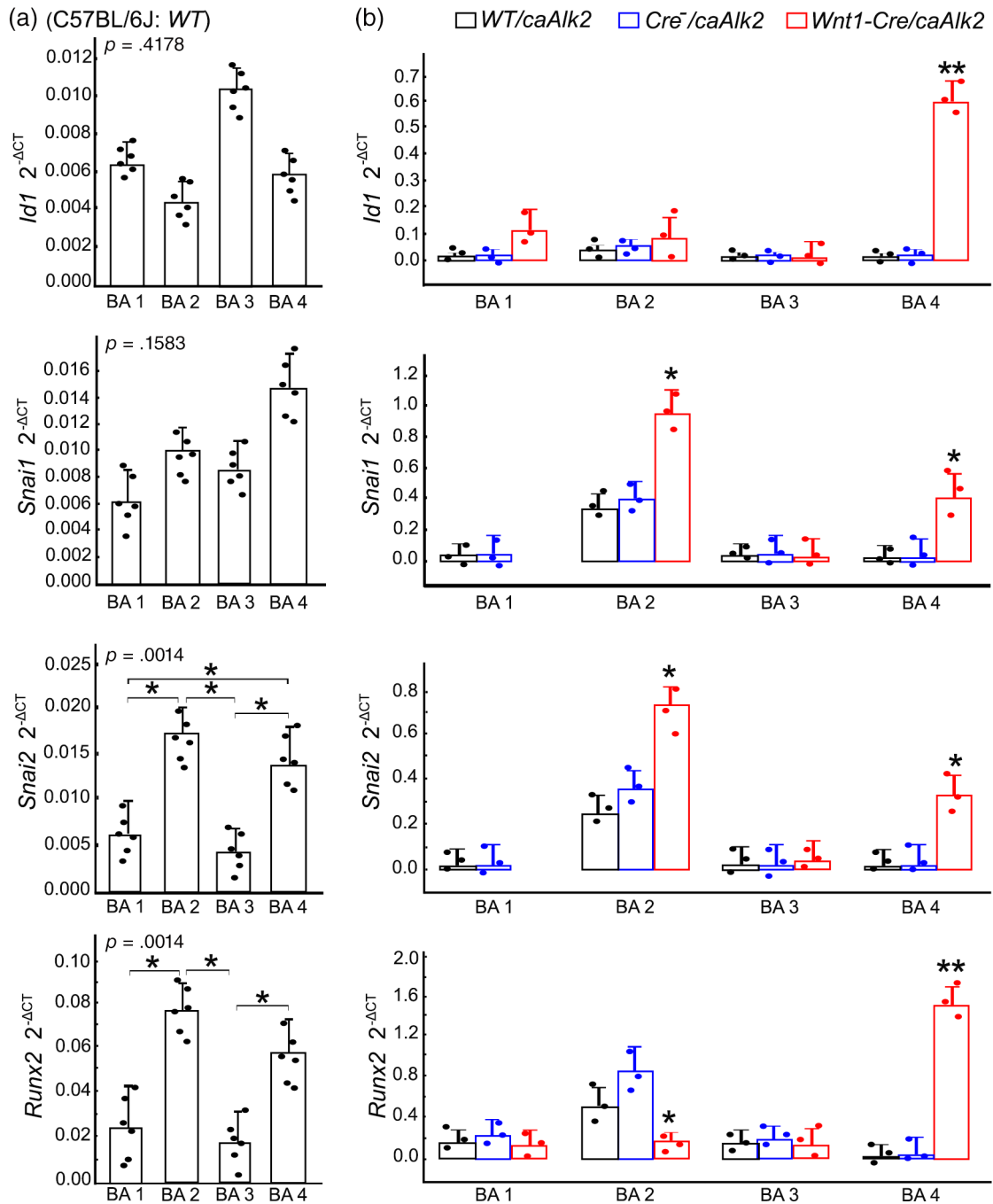
FIGURE 6 Quantitative RT-PCR of bone morphogenetic protein (BMP) target genes in branchial arches of E10.5 _C57BL/6J_ wild type (WT, a); _Wnt1-Cre/caAlk2_ mutant, _Cre⁻/caAlk2_ littermate control and _C57BL/6J_ WT/caAlk2 (b) embryos. Histograms represent means ± standard deviation ($X \pm SD$) of $2^{-\Delta CT}$ values of examined BMP target genes (_Id1_, _Snai1_, _Snai2_, and _Runx2_) in individual branchial arches (BAs) of _C57BL/6J_ WT (a; $n = 6$), _C57BL/6J WT/caAlk2_ (black bars in b; $n = 3$), _Cre⁻/caAlk2_ littermate control (blue bars in b; $n = 3$) and _Wnt1-Cre/caAlk2_ (red bars in b; $n = 3$) mice. $*p \le .05$ (a) one-way ANOVA followed by Fisher's least significant difference (LSD) analyses. $*p \le .05$, $**p \le .01$ (b) compared to corresponding BAs of _Cre⁻/caAlk2_ littermate control using two-way ANOVA followed by Fisher's LSD analyses

lamina propria—a zone of loose connective tissue under the epithelium, in both littermate controls (Figure 4a and inset, arrowheads) and _Wnt1-Cre/caAlk2_ mutants (Figure 4b and inset, arrowheads). E-Cadherin⁺ epithelium was progressively thinner along the anteroposterior axis in the dorsal surface of oral tongue of E18.5 _Wnt1-Cre/caAlk2_ mutants (Figure 4d and inset, arrowhead) compared to that of littermate controls (Figure 4c and inset, arrowhead).

Fungiform taste papillae were not as well developed in the E18.5 _Wnt1-Cre/caAlk2_ mutant tongues (arrow in inset of Figure 4d) as those in the littermate controls (arrow in inset of Figure 4c). Further, Spine-like filiform papillae were not as evident in the _Wnt1-Cre/caAlk2_ mutant tongues (open arrowhead in inset of Figure 4d) as that of littermate control tongues (open arrowhead in inset of Figure 4c). Defects in muscle differentiation and organization were examined using muscle
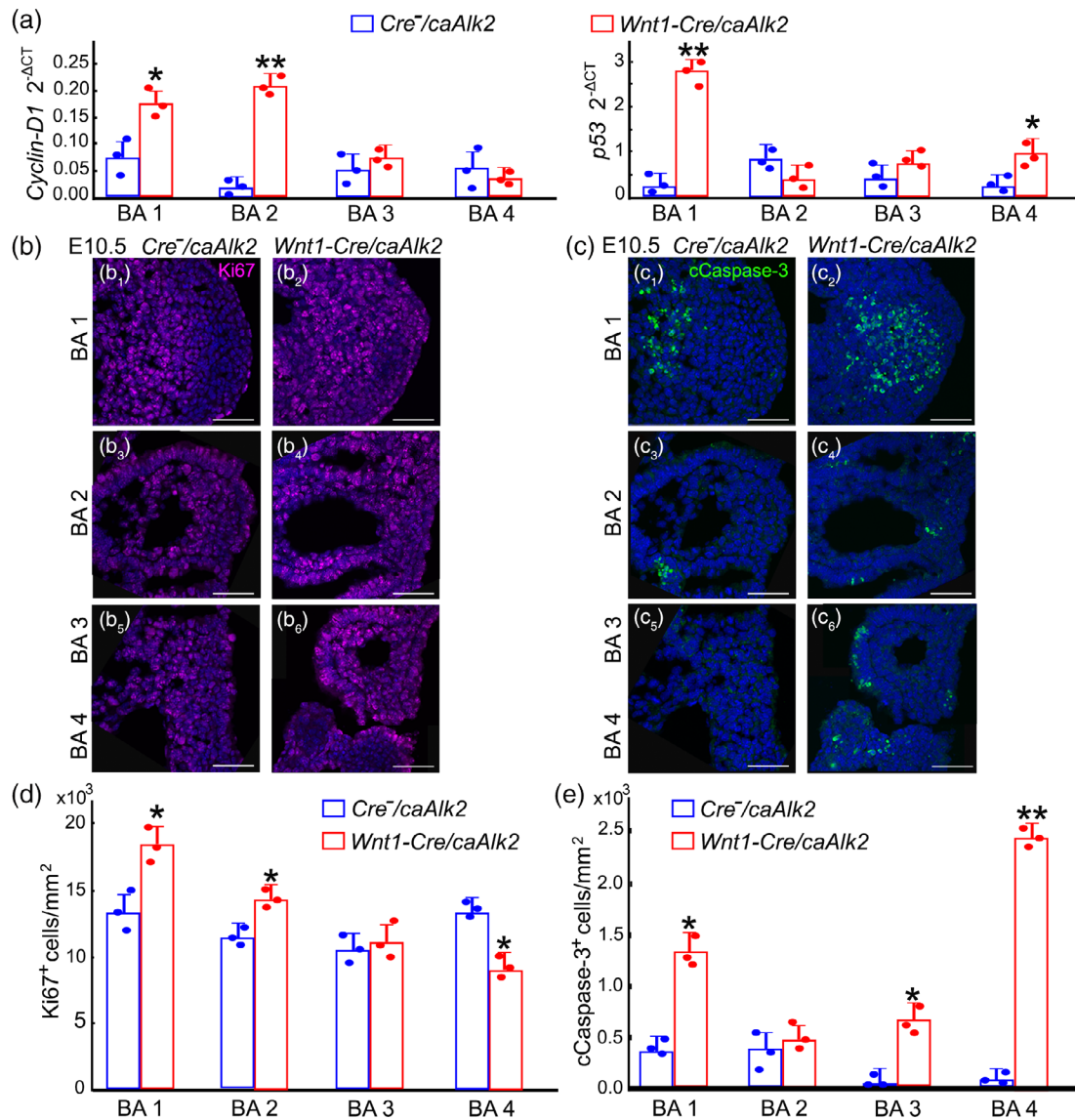
FIGURE 7 Effects of elevated ALK2-BMP signaling on cell proliferation and apoptosis in E10.5 branchial arches (BAs). (a) Histograms ($X \pm SD$; $n = 3$) of $2^{-\Delta CT}$ values of cell proliferation associated gene *Cyclin-D1* and apoptosis associated gene *p53* in individual BAs of *Wnt1-Cre/caAlk2* and *Cre$^-$/caAlk2* littermate control. *$p \leq .05$, **$p \leq .01$ compared to the corresponding BA of littermate control using two-way ANOVA followed by Fisher's least significant difference (LSD) analyses. (b, c) Single-plane laser scanning confocal images of transverse BA sections immunostained with cell proliferation marker Ki67 (b, magenta) or apoptosis marker cleaved (c) Caspase-3 (c, green) in littermate control (b_1, b_3, b_5/c_1, c_3, c_5) and *Wnt1-Cre/caAlk2* (b_2, b_4, b_6/c_2, c_4, c_6) mice. Scale bars: 50 μm. (d, e) Histograms ($X \pm SD$; $n = 3$) of the total number of Ki67$^+$ cells per mm^2 (d) or cCaspase-3$^+$ cells per mm^2 (e) in individual BAs of littermate controls and *Wnt1-Cre/caAlk2* mutants. *$p \leq .05$, **$p \leq .01$ compared to the corresponding BA of littermate control using two-way ANOVA followed by Fisher's LSD analyses

specific marker Desmin. All four intrinsic glossal muscles were disorganized in the E18.5 *Wnt1-Cre/caAlk2* mutants (Figure 4f,f$_1$) compared to littermate controls (Figure 4e,e$_1$). Superior and inferior longitudinal muscles that are close to the dorsal and ventral tongue surface (Figure 4e$_1$, sLG, iLG) were not apparent in the *Wnt1-Cre/caAlk2* mutants (Figure 4f$_1$). Transverse muscles (Figure 4e$_1$, Tr) were sparse and largely empty in the space for their distribution in *Wnt1-Cre/ caAlk2* mutants (Figure 4f$_1$, Tr). In contrast, vertical muscles (Figure 4e$_1$, Ve) were increased in bundle size in the middle region of the tongue in *Wnt1-Cre/caAlk2* mutants (Figure 4f, Ve).

2.4 | Tongue primordia (i.e., branchial arches) developed deficiently in E10.5 *Wnt1-Cre/caAlk2* mutants

To understand the cause of microglossia in *Wnt1-Cre/caAlk2* mutants, the development of tongue primordia (i.e., BAs 1–4) was examined. *Wnt1-Cre* marked *RFP* signals were distributed in BAs 1–4 (Figure 5a$_1$, arrowheads) at E10.5. RFP$^+$ cells were under E-cadherin$^+$ epithelium and exclusively present in the mesenchyme (Figure 5a$_2$–a$_6$).

An elevated activation of ALK2-BMP signaling was validated by detecting the phosphorylation of Smads. Phosphorylated (p)-Smad1/5/8

known to mediate BMP signaling was detected at a higher level in BAs of E10.5 *Wnt1-Cre/caAlk2* mutants compared to *Cre⁻/caAlk2* littermate controls (595.02 ± 17.56 vs. 155.29 ± 6.26 in mean gray scale intensity, $p < .01$ in Figure 5b). In contrast, the level of p-Smad2/3, that is, known to mediate TGF-β signaling (Grönroos et al., 2012) was not apparently altered in *Wnt1-Cre/caAlk2* mutants (82.56 ± 11.65 vs. 71.98 ± 4.49 in mean gray scale intensity, $p > .05$ in Figure 5b). On sections, mesenchymal cells that were positive for p-Smad1/5/8 immunosignals were significantly increased ($p < .01$; Figure 5d) in each of BAs 1–4 of E10.5 *Wnt1-Cre/caAlk2* mutants (Figure $5c_4$–c_6,d) compared to littermate controls (Figure $5c_1$–c_3,d). Further, an alteration of mesenchymal cell density in BA 1 (increase) and BA 4 (decrease) was observed in the E10.5 *Wnt1-Cre/caAlk2* mutants ($p < .05$; Figure 5d).

All four BAs ($n = 18$) were developed, and from the side view of BAs 1–4 there were no obvious differences between *Wnt1-Cre/caAlk2* mutants (Figure $5e_2$) and littermate controls (Figure $5e_1$). However, dorsal view showed that BA 1 had a flat dorsal surface in E10.5 *Wnt1-Cre/caAlk2* mutants (Figure $5f_2$, arrowhead) in contrast to the profound swelling in littermate controls (Figure $5f_1$, arrowhead). An enlarged copula was observed in *Wnt1-Cre/caAlk2* mutant BA 2 (Figure $5f_2$, arrow) compared to that of the *Cre⁻/caAlk2* littermate control (Figure $5f_1$, arrow).

2.5 | BAs 1-4 exhibited distinct gene expression and changes in *Wnt1-Cre/caAlk2* mutants

To understand the downstream factors that are mediating the tongue region-specific effects of elevated ALK2-BMP signaling, individual BAs were separated under a microscope at the clear boundaries between BAs, and transcripts of BMP target genes for cell growth (*Id1*, *Snai1*, *Snai2*, and *Runx2*) were analyzed in E10.5 *C57BL/6J* wild type (WT), *Wnt1-Cre/caAlk2* mutants and *Cre⁻/caAlk2* littermate controls. Overall, individual BAs showed different gene expression levels and alterations (Figure 6a). Out of the four tested BMP target genes, levels of *Snai2* and *Runx2* were significantly different ($p < .01$) among BAs 1–4 in E10.5 *C57BL/6J* WT embryos (Figure 6a). No significant changes in *Id1* and *Snai1* expression levels were observed within any of the E10.5 WT BAs. In contrast to those in littermate controls, gene expression levels were altered in *Wnt1-Cre/caAlk2* mutant BAs (Figure 6b). Specifically, compared to *Cre⁻/caAlk2* littermate controls, *Wnt1-Cre/caAlk2* mutants had: (a) no detected level of *Snai1* and *Snai2* expression in BA 1 of *Wnt1-Cre/caAlk2* mutants; (b) increased *Snai1 and Snai2*, and decreased *Runx2* in BA 2 ($p < .05$; Figure 6b); (c) significantly higher mRNA levels of all the BMP target genes tested in BA 4 ($p < .05$); (d) no alterations of gene expression in BA 3 (Figure 6b; $p > .05$).

Of note, differences of BMP target gene expression in E10.5 BAs were detected between *C57BL/6J* WT and *Cre⁻/caAlk2* littermate controls. To understand whether the discrepancies were caused by the transgene insertion, *C57BL/6J* WT were bred with *caAlk2* to generate *caAlk2* heterozygotes (*C57BL/6J WT/caAlk2*) for analyses of the gene expression in BAs. Of all the BMP target genes tested, the expression patterns in *C57BL/6J WT/caAlk2* BAs (Figure 6b) resembled those in *Cre⁻/caAlk2* littermates (Figure 6b) and were different from those in *C57BL/6J* WT controls (Figure 6a).

To understand the relevance of cell proliferation and apoptosis with the posteriorly truncated microglossia in *Wnt1-Cre/caAlk2* mutants, transcripts of proliferation relevant gene *Cyclin-D1* and key apoptosis gene *p53* in individual BAs were analyzed in E10.5 *Wnt1-Cre/caAlk2* mutants and *Cre⁻/caAlk2* littermate controls (Figure 7a). Increased gene expression of *Cyclin-D1* was detected in BAs 1 ($p < .05$; Figure 7a) and 2 ($p < .01$; Figure 7a), whereas *p53* expression levels were higher in BAs 1 ($p < .01$) and 4 ($p < .05$) of *Wnt1-Cre/caAlk2* mutants compared to the corresponding *Cre⁻/caAlk2* littermate control BAs (Figure 7a). No significant changes in *Cyclin-D1* expression were observed in BA 3–4 in E10.5 *Wnt1-Cre/caAlk2* mutants ($p > .05$; Figure 7a) compared to *Cre⁻/caAlk2* littermate controls (Figure 7a). Similarly, no significant changes in *p53* expression were observed in BA 2–3 in E10.5 *Wnt1-Cre/caAlk2* mutants ($p > .05$; Figure 7a) compared to *Cre⁻/caAlk2* littermate controls (Figure 7a). Ki67⁺ proliferating cells were more densely distributed per unit area (mm^2) in BA 1 and 2 of E10.5 *Wnt1-Cre/caAlk2* mutants (Figure $7b_2$,b_4, $p < .05$ in d) than that of *Cre⁻/caAlk2* littermate controls (Figure $7b_1$,b_3,d). In contrast, the density of Ki67⁺ proliferating cells was decreased in BA 4 of *Wnt1-Cre/caAlk2* mutants (Figure $7b_6$, $p < .05$ in d) compared to the *Cre⁻/caAlk2* littermate control BA 4 (Figure $7b_5$,d). No obvious changes in Ki67⁺ cells were detected in the BA 3 of *Wnt1-Cre/caAlk2* mutants (Figure $7b_6$, $p > .05$ in d) compared to those of *Cre⁻/caAlk2* littermate controls (Figure $7b_5$,d). Further, mesenchymal cells marked by immunosignals of apoptotic cell marker cleaved (c) Caspase-3 were significantly higher in E10.5 BA 1, 3, and 4 of *Wnt1-Cre/caAlk2* mutants (Figure $7c_2$,c_6, $p < .05$ in e) than corresponding BAs of *Cre⁻/caAlk2* littermate controls (Figure $7c_1$,c_5,e). However, no significant changes in cCaspase-3⁺ cells was observed in *Wnt1-Cre/caAlk2* mutant BA 2 (Figure $7c_4$, $p > .05$ in e) compared to the *Cre⁻/caAlk2* littermate control BA 2 (Figure $7c_3$,e).

3 | DISCUSSION

Our present study demonstrated that elevated ALK2-BMP signaling in neural crest and derived mesenchyme leads to posteriorly truncated microglossia and disorganized lingual tissues. The more severe tongue deformity along the anteroposterior axis and distinct alterations of gene expression and cell behavior in BAs 1–4 of *Wnt1-Cre/caAlk2* mutants indicate that neural crest-derived mesenchymal cells in BAs 1–4 respond to elevated ALK2-BMP signaling in a region-specific manner. Overall, our results indicated that appropriate levels of ALK2-BMP signaling activity in neural crest-derived mesenchyme plays essential roles in coordinating various tissue and cell types for the proper formation of the tongue organ and its epithelial appendages (e.g., taste papillae and taste buds). The phenotype is severe and different from the mild defect resulted from the elevated ALK3-BMP signaling activity (Li et al., 2013), which indicates distinct roles of specific receptor-mediated BMP signaling in the tongue organogenesis.

3.1 | Appropriate levels of ALK2-BMP signaling activity in neural crest and the derived lingual mesenchyme is required for proper tongue organogenesis

The neural crest is a multipotent cell population derived from the lateral ridges of the neural plate in early vertebrate embryos (Leikola, 1976; Trainor, 2015). In mice, cranial neural crest cells populate directly under the epithelium of the tongue primordium (branchial arch 1) as early as 1–2 somite stages (E8.0–8.5; Serbedzija, Bronner-Fraser, & Fraser, 1992). Neural crest-derived cells are extensively distributed in the mesenchyme/connective tissue of the tongue (Boggs et al., 2016; Liu, Komatsu, et al., 2012; Thirumangalathu et al., 2009) and are regarded as scaffolds of the tongue organ (Chai & Maxson, 2006; Cordero et al., 2011). Structural and molecular disruption of neural crest and neural crest-derived cells causes severe defects in tongue formation. For instance, lacking primary cilia in neural crest cells causes aglossia (Millington et al., 2017). Deficient molecular signaling of Wnt (Liu et al., 2009; Liu, Grosse, et al., 2012; Zhong, Zhao, Mayo, & Chai, 2015; Zhu et al., 2017) and TGF-β (Iwata et al., 2013) result in microglossia due to defects in cells migrating into and surviving in the tongue anlage. Our study in demonstration of the importance of ALK2-BMP signaling in neural crest and derived mesenchymal cells in the tongue formation suggest that organogenesis of the tongue involves a complex network of molecular signaling pathways. Detection of an increased p-Smad1/5/8 and unchanged p-Smad2/3 level in the E10.5 Wnt1-Cre/caAlk2 mutant BAs confirmed that the intracellular cascades of ALK2-BMP signaling were through p-Smad1/5/8 that is separate from TGF-β signaling that utilizes p-Smad2/3 (Grönroos et al., 2012). Moreover, our observations of an uneven severity of tongue development in Wnt1-Cre/caAlk2 mutants suggest that tongue formation is finely tuned in a region-specific manner.

To understand the progressively increased severity of tongue deformity along the anteroposterior axis, we detected expression levels of genes in individual BAs including BMP target genes associated with cell growth (Id1, Snai1, Snai2, and Runx2), cell proliferation regulating gene (Cyclin-D1) and apoptosis control gene (p53) in Wnt1-Cre/caAlk2 mutant, Cre⁻/caAlk2 littermate control and C57BL/6J wild type (WT) mice. Individual BAs had significantly different expression levels of BMP target genes Snai2 and Runx2 in E10.5 C57BL/6J WT embryos suggesting distinct levels of BMP signaling activity. Moreover, alterations of gene expression levels in each BA of Wnt1-Cre/caAlk2 mutants were different suggesting that individual BAs respond to elevated ALK2-BMP signaling distinctly. BA 4 was most responsive such that all tested BMP target genes were altered. Ultimately, a significantly lower cell proliferation in BA 4 and higher apoptosis in BA 3 and 4 (Pietsch, Sykes, McMahon, & Murphy, 2008) might be the cause of the decreased cell number in BA 4 mesenchyme and absence of pharyngeal tongue since BAs 3–4 are the main contributor to the formation of pharyngeal tongue (Cobourne et al., 2018; Parada, Han, & Chai, 2012). Differences of BMP target gene expression pattern in E10.5 BAs were detected between C57BL/6J WT and

Cre⁻/caAlk2 littermate controls. This was confirmed by the data from an independent experiment in caAlk2 hemizygous embryos through crossing with C57BL/6J WT breeders. Although we do not have evidence-based explanations, this discrepancy of gene expressions might be caused by (a) the genetic background difference—since caAlk2 mice are maintained mixture of 129S6 and C57BL/6J, and (b) alterations in gene expressions by transgene insertion, which is not uncommon. However, these Cre⁻/caAlk2 littermate controls did not exhibit phenotypic alterations demonstrating that the phenotypes we observed in Wnt1-Cre/caAlk2 mutants were due to the activation of caAlk2.

We observed a significantly higher level of p53 transcripts and more apoptotic cells in BA 1 of Wnt1-Cre/caAlk2 mutants, however, the cell proliferation regulating gene Cyclin-D1 (Yang, Hitomi, & Stacey, 2006) as well as cell proliferation were increased in BA 1–2. A promoted cell proliferation in the mutant BA 1 and 2 may overwrite the cell death and be responsible for the formation of the small oral tongue to which BA 1 and a portion of BA 2 contribute (Cobourne et al., 2018; Parada et al., 2012). This is supported by the increased cell count in the mesenchyme of mutant BA1.

Interestingly, we noticed that even though Wnt1-Cre labeled most, if not all, of the cells in the mesenchyme of BAs 1–4, only a population of mesenchymal cells had promoted cell proliferation or apoptosis. The data indicate that the mesenchymal cells in BAs responded to elevated ALK2-BMP signaling activity distinctly.

In summary, our data showed that expression levels of BMP target genes are distinct among individual BAs and that neural crest and the derived mesenchymal cells in individual BAs respond differentially in gene expression and cell behaviors to the constitutive activation of ALK2-BMP signaling. The results suggest that distinct levels of ALK2-BMP signaling activity in individual BAs are required for the cell behavior and functions during normal tongue development.

3.2 | ALK2-BMP signaling regulates the interactions of neural crest-derived mesenchyme with other lingual tissues for their proper development and organization

As aforementioned, the tongue is comprised of multiple tissues that are connected by the mesenchyme/connective tissue arising primarily from neural crest and serving as a scaffold of the organ (Rinon et al., 2007). The neural crest-derived tongue mesenchyme compartmentalizes lingual muscles and allows nerves and blood vessels to traverse through. In the present study, we provide evidence for an important role of mesenchymal ALK2-BMP signaling in regulating the development of multiple tissues in the tongue. Constitutive activation of ALK2-BMP signaling in tongue mesenchyme led to altered orientation of muscle fibers, reduced branching and growth of nerves, thinner epithelium and arrest of further development of fungiform papillae and taste buds at late embryonic stages.

During the initial formation of the tongue organ, neural crest and neural crest-derived cells migrate into the tongue primordium before myogenic progenitors (Parada et al., 2012), and it has been speculated that neural crest-derived cells in the tongue mesenchyme acts as a

niche that release molecular instructions to direct survival, proliferation, and differentiation of myogenic progenitors as well as the patterning of the muscle (Parada et al., 2012; Parada & Chai, 2015). In the present study, we observed missing of muscle fibers at certain orientations (e.g., longitudinal and transverse muscle fibers) in *Wnt1-Cre/caAlk2* mutant mice suggesting that ALK2-BMP signaling regulate how mesenchymal cells interact and guide myogenic processes and patterning.

In addition to the defects of muscle cells in *Wnt1-Cre/caAlk2* mutants, there were also changes in the nerve outgrowth and branching. Although nerve fibers were not tracked to distinguish the gustatory (chorda tympani) from somatosensory (trigeminal) innervating fibers, we observed that *Wnt1-Cre/caAlk2* mutant tongues lack βIII-tubulin$^+$ nerve fibers in the vicinity of taste papillae and surrounding epithelium at E14.5, within early fungiform taste buds and surrounding epithelium at E18.5. The results indicate that both nerves were affected by the elevated ALK2-BMP signaling in tongue mesenchyme. Glial cells including the myelinating Schwann cells are derived from neural crest (Mayor & Theveneau, 2013). Our results support the idea that ALK2-BMP signaling is involved in regulating the interactions of neural crest-derived stromal and/or Schwann cells with axons for proper nerve outgrowth, pathfinding, and/or branching.

The development of epithelial appendages requires the interactions with the underlying mesenchyme (Thesleff, 2003). Both direct (Ribatti & Santoiemma, 2014) and indirect (Jussila & Thesleff, 2012) cell–cell interactions between mesenchymal and epithelial cells have been reported. Multiple signaling pathways are involved in the mesenchymal–epithelial interactions (Puthiyaveetil, Kota, Chakkarayan, Chakkarayan, & Thodiyil, 2016), among which BMP signaling plays important roles (Merrill, Eames, Weston, Heath, & Schneider, 2008). Profound effects of BMPs (2, 4, and 7) and antagonists (noggin and follistatin) in taste papilla formation and patterning have been reported (Beites et al., 2009; Zhou et al., 2006). Here, we provide evidence that ALK2 is a mediating receptor of BMP signaling in lingual mesenchyme for its interactions with other tissues.

Moreover, our results showed that *Wnt1-Cre/caAlk2* mutants had well-formed fungiform papillae on the small tongue, however at E18.5 tongue epithelium became thinner and further development of fungiform papillae and taste buds were arrested. The data indicate that appropriate level of ALK2-BMP signaling is critical in mesenchymal interactions with the overlying epithelium for epithelial cell proliferation and differentiation, thus advancing fungiform papilla development. It is noteworthy that early taste buds were formed in the less advanced fungiform papillae without innervation, indicating that taste bud formation and cell differentiation are nerve-independent which is also supported by other reports (Castillo et al., 2014; Farbman & Mbiene, 1991; Fritzsch, Sarai, Barbacid, & Silos-Santiago, 1997; Ito, Nosrat, & Nosrat, 2010; Mbiene et al., 1997; Ren et al., 2017). However, lack of innervation might be one of the causes for the arrest of further development of fungiform taste buds observed in E18.5 mutant tongues. Further, our observation that the *Wnt1-Cre/caAlk2* mutants had an enlarged Shh$^+$ patch of tissue that was presumably a circumvallate papilla placode at E12.5 but lacked a circumvallate taste papilla at E14.5 indicates that the circumvallate is initially specified but eventually is not sustained. It is possible that the pharyngeal tongue region is important for sustaining the development of the circumvallate papilla.

Collectively, our data provide evidence that ALK2-BMP signaling in neural crest-derived mesenchyme regulates mesenchymal interactions with other lingual tissues including epithelium, muscles, and nerves for their development and organization. Since Type I BMP receptors are present in both tongue epithelium and mesenchyme (Beites et al., 2009; Jung et al., 1999; Kawasaki et al., 2012; Li et al., 2013; Suga et al., 2007; Zhou et al., 2006), further studies are needed to understand the specific roles of each receptor in distinct tissue compartments.

4 | MATERIALS AND METHODS

4.1 | Mouse lines and tissue collection

The animal use was approved by the institutional animal care and use protocols of the University of Georgia and in accordance with National Institute of Health guidelines for proper care and use of animals for research. Mice carrying constitutively activated form of Type I BMP receptor *Alk2* (CAG-Z-EGFP-caAlk2) transgene (hereafter *caAlk2*) were provided by Dr. Yuji Mishina, University of Michigan (Fukuda et al., 2006). Heterozygous *Wnt1-Cre* mice [B6.Cg-Tg (Wnt1-Cre) 11Rth Tg(Wnt1-GAL4) 11Rth/J, Jackson Laboratory, Stock# 009107] were bred with homozygous *caAlk2* breeders to generate the *Wnt1-Cre/caAlk2* mice. Homozygous RFP mice [B6.Cg-Gt (ROSA)26 Sortm14(CAG-tdTomato)Hze/J, The Jackson Laboratory, Stock# 007914] were used as the reporter to bred with *Wnt1-Cre* breeders to generate *Wnt1-Cre/RFP* mice. Wild type (*C57BL/6J*, Jackson Laboratory, Stock# 000664) mice were used to cross with homozygous *caAlk2* breeders to generate the *C57BL/6J WT/caAlk2* mice.

Littermates that were negative for *Wnt1-Cre* were used as controls (*Cre$^-$/caAlk2*). Genotype of mice was confirmed using specific primers. PCR product of Cre (200 bp) were identified using primers CreF (5′-CTC GTG ATC TGC AAC TCC AGTC-3′) and CreR (5′-GAG ACT AGT GAG ACG TGC TACT-3′). PCR products of *caAlk2* (580 bp) were identified using primers TF41 (5′-GTG CTG GTT ATT GTG CTG TCTC-3′) and TF61 (5′-TGT GAG CGA GTA GTA ACA ACC-3′). PCR product of RFP (200 bp) were identified using primers oIMR9103 (5′-GGC ATT AAA GCA GCG TAT CC-3′) and oIMR9105 (5′-CTG TTC CTG TAC GGC ATG G-3′).

Timed pregnant mice were euthanized using CO_2 followed by cervical dislocation for embryonic tissue collection. Embryos were harvested at E10.5, E12.5, E14.5, E16.5, and E18.5. Noon of the day of vaginal plug detection was designated as embryonic day 0.5 (E0.5). All embryo dissections were performed between 12.00 p.m. and 3.00 p.m. for consistency across litters. The uterus with embryos was removed and embryos were retrieved under a microscope. Stages of the embryos were confirmed by the number of somite pairs and development of multiple organs. Dissected tissues were further processed for different analyses as described below.

4.2 | Whole mount immunohistochemistry

Immunohistochemistry against Sonic Hedgehog (Shh), a developing papilla marker, was performed on whole tongue on the mandible (E12.5, E14.5) using goat polyclonal, affinity-purified antibody against mouse Shh N-terminal peptide [amino acids 25–198] (AF464, R&D Systems, Minneapolis, MN) as previously described (Liu et al., 2004; Mistretta, Liu, Gaffield, & MacCallum, 2003; Zhou et al., 2006). E12.5 and E14.5 tongues with mandibles were fixed in 4% paraformaldehyde (PFA) in 0.1 M PBS, at 4°C for 2 hr, then transferred to 100% methanol for storage at −20°C until use.

Tongues were treated with 6% H_2O_2 in 100% methanol at room temperature for 5 hr to block endogenous peroxidase activity followed by rehydration through a descending methanol series (50, 25, and 0% in 0.1 M PBS) at room temperature for 30 min each. Antigen retrieval was performed by heating the tissues at 92–95°C for 5 min in Universal Antigen Retrieval Agent (CTS015; R&D Systems, Minneapolis, MN). PBS/MT (0.1 M PBS with 2% skim milk powder and 0.1% Triton X-100) was used to block nonspecific staining. Tongues were then incubated with primary antibody at a 1:300 dilution in 10% normal donkey serum (NDS; D9663; Sigma Aldrich, St Louis, MO) in PBS/MT at 4°C for 48 hr. After rinses with PBS/MT (five times, 1 hr each on ice) tissues were incubated at 4°C for 24 hr with biotin-conjugated rabbit anti-goat secondary antibody (1:500, BA-5000; Vector Laboratories, Burlingame, CA) in 1% NDS in PBS/MT. Following the rinses with PBS/MT (five times, 1 hr each on ice), tongues were incubated at 4°C for 24 hr with peroxidase-conjugated streptavidin in blocking solution (1:500, PK6200; Vector Laboratories, Burlingame, CA). After five rinses in PBS/MT and two rinses in PBT (0.1 M PBS with 0.1% Triton X-100 and 0.2% bovine serum albumin) for 1 hr each on ice, tongues were preincubated in nickel-intensified DAB solution (SK4100; Vector Laboratories, Burlingame, CA) without H_2O_2 at room temperature for 30 min followed by incubation with DAB solution containing 0.0003% H_2O_2. The reaction was stopped by PBS rinses twice for 1 hr each. Tongues were then transferred into 4% PFA in 0.1 M PBS at 4°C for further fixation and photographed in PBS.

4.3 | Immunohistochemistry on sections

Embryos were fixed with 4% PFA in 0.1 M PBS at 4°C for 2 hr, cryoprotected in 30% sucrose at 4°C for 48 hr, then embedded in OCT (#23730571; Fisher Scientific, Waltham, MA) and rapidly frozen. Serial sections were cut at 10 μm in thickness. Sections were air-dried, rehydrated, and blocked with 10% NDS in PBS-X (0.1 M PBS, 0.3% Triton X-100) at room temperature for 1 hr. Primary antibodies listed in Table 1 were diluted in PBS-X containing 1% NDS (carrier solution). Sections incubated with carrier solution without primary antibody were used as negative controls.

After incubation with primary antibodies at 4°C for 24 hr, sections were washed three times with 0.1 M PBS, and then incubated with secondary antibodies conjugated with Alexa Fluor 488, or 647 (1:500, Jackson immune research, West Grove, PA) in carrier solution at room temperature for 1 hr. After rinsing in PBS, sections were counterstained with DAPI solution (200 ng/ml in PBS, D1306; Life Technologies, Carlsbad, CA) at room temperature for 10 min. After thorough rinsing in PBS, the sections were air-dried and mounted with ProLong® Diamond antifade medium (P36970; Fisher Scientific, Waltham, MA).

4.4 | Early taste bud labeling with keratin 8 (K8) immunosignals on epithelial sheets

Peeling of epithelial sheets from E18.5 tongues of *Wnt1-Cre/caAlk2* mutants and *Cre⁻/caAlk2* littermate controls was performed as previously described (Venkatesan, Boggs, & Liu, 2016). A mixture of collagenase A (1 mg/ml, #10103578001; Roche Diagnostics, Basal, Switzerland) and dispase II (2.5 mg/ml; # 10374300; Roche Diagnostics, Basal, Switzerland) in 0.1 M PBS was injected into the subepithelial space of E18.5 *Wnt1-Cre/caAlk2* mutant and littermate control tongues. After the injection, tongues were incubated at 37°C for 30 min followed by fixation in 4% PFA in 0.1 M PBS at room temperature for 1 hr. The epithelial sheet of the tongue was separated from the lamina propria and then rinsed three times in 0.1 M PBS at room temperature for 30 min each.

Following the incubation with 10% NDS in PBS-X at room temperature for 1 hr to block nonspecific staining, the epithelial sheets

TABLE 1 Primary antibodies used for immunohistochemistry

Primary antibody	Source (catalog number, company)	Dilution
Goat anti Shh	AF464, R&D systems, Minneapolis, MN	1:300
Rabbit anti p-Smad1/5/8	#13820, Cell signaling, Danvers, MA	1:1,000
Rabbit anti p-Smad2/3	#3101, Cell signaling, Danvers, MA	1:1,000
Mouse anti GAPDH	G8795, Sigma Aldrich, St Louis, MO	1:10,000
Rabbit anti βIII-tubulin	ab18207, Abcam, Cambridge, United Kingdom	1:1,000
Chicken anti Vimentin	AB5733, EMD millipore, Burlington, MA	1:1,000
Rabbit anti Desmin	ab15200, Abcam, Cambridge, United Kingdom	1:1,000
Goat anti E-cadherin	AF748, R&D systems, Minneapolis, MN	1:1,000
Rat anti keratin 8	TROMA-I, Developmental Studies Hybrydoma Bank, Iowa city, IA	1:1,000
Sheep anti Ki67	AF7649, R&D systems, Minneapolis, MN	1:500
Rabbit anti cCaspase-3	#9661, Cell signaling, Danvers, MA	1:500

were incubated with primary antibody against K8 in carrier solution at 4°C for 48 hr. After three rinses in 0.1 M PBS at room temperature for 30 min each, epithelial sheets were incubated at 4°C for 24 hr with Alexa Fluor 647-conjugated donkey anti-rat secondary antibody (1:500, #712-605-150; Jackson ImmuneResearch, West Grove, PA) in carrier solution. The epithelial sheets were rinsed with 0.1 M PBS and transformed into 4% PFA in 0.1 M PBS at 4°C for further fixation and photographed in PBS.

4.5 | RNA extraction and quantitative reverse transcriptase polymerase chain reaction (RT-PCR)

Individual branchial arches (BAs) (1–4) from *Wnt1-Cre/caAlk2* mutants and *Cre⁻/caAlk2* littermate controls were dissected at E10.5 and immersed in Trizol (#15596018; Life technologies, Carlsbad, CA) solution for RNA extraction. A total of nine tissues (pooled three tissues x three replicates) were used from each BA for RNA extraction. Tissues were homogenized with a PorGen 700D tissue homogenizer (Fisher Scientific, Waltham, MA) and RNA was extracted using the RNeasy Plus kit (#74136; Qiagen, Hilden, Germany). RNA concentrations were determined using Nanodrop 8000 spectrophotometer (Nanodrop, Thermo Scientific, Waltham, MA). Complementary DNA was synthesized from the RNA extracts using SuperScript™ First-Strand Synthesis System (#11902018; Fisher scientific, Waltham, MA). The cDNA products were used to analyze the expression of selected genes using the primers in Table 2.

4.6 | Western blotting

Proteins were extracted from the mesenchyme using Radio-immunoprecipitation assay buffer/RIPA buffer (1% NP-40, 150 mmol/L NaCl, 50 mmol/L Tris-HCl, 0.5% sodium deoxycholate, 0.1% SDS, 1 mmol/L EDTA, pH 7.4). The epithelium was removed from E10.5 BAs of *Wnt1-Cre/caAlk2* mutant (n = 3) and *Cre⁻/caAlk2* littermate control (n = 3) mouse embryos as previously described (Liu, Henson, Zhou, D'Silva, & Mistretta, 2008). Protein concentrations were determined using Pierce™ BCA protein assay kit (#23225; Thermo Fisher Scientific, Waltham, MA) and Synergy™ 4 microplate reader (#7161000; BioTek Instruments, Winooski, VT). Protein extracts were then resolved using sodium dodecyl sulfate–polyacrylamide gel electrophoresis (SDS-PAGE) and transferred to nitrocellulose membranes. Membranes were blocked with 3% bovine serum albumin (A-420-100; Gold Biotechnology, St Louis, MO) in tris-buffered saline with Tween 20 buffer/TBST buffer (20 mM Tris pH 7.5, 150 mM NaCl, 0.1% Tween 20) at room temperature for 1 hr. The membranes were incubated with primary antibodies (Rabbit anti p-Smad1/5/8, rabbit p-Smad2/3, and GAPDH; Table 1) in blocking buffer (3% BSA in TBST) at 4°C for 24 hr. After three rinses in TBST (10 min each), membranes were incubated with Alexa Fluor 647-conjugated goat anti-rabbit (1:10,000, #711-605-152, Jackson Immunoresearch, West Grove, PA) and Alexa Fluor 647-conjugated donkey anti-mouse (1:10,000, #715-605-150, Jackson Immunoresearch, West Grove, PA) secondary antibodies in blocking buffer at room temperature for 2 hr. Band detection was performed using chemiluminescence (ChemiDoc^MP Imaging System, Bio-Rad ChemiDoc, Hercules, CA).

TABLE 2 Primer sequences used for the quantitative reverse transcriptase polymerase chain reaction (qRT-PCR)

Gene	Primer sequence
Id1	Forward 5′ GAG TCT GAA GTC GGG ACC AC 3′ Reverse 5′ CCT CAG CGA CAC AAG ATGC 3′
Snai1	Forward 5′ CTT GTG TCT GCA CGA CCT GT 3′ Reverse 5′ CTT CAC ATC CGA GTG GGT TT 3′
Snai2	Forward 5′ GGC TGC TTC AAG GAC ACA TT 3′ Reverse 5′ TTG GAG CAG TTT TTG CAC TG 3′
Runx2	Forward 5′ AAG AAG AGC CAG GCA GGT GC 3′ Reverse 5′ CAT ACC GAG GGA CAT GCC TGAG 3′
Cyclin D1	Forward 5′ GAC GGC GTC AAA TAT GTC CT 3′ Reverse 5′ CTG GAG AGT GAC AGC ATG GA 3′
p53	Forward 5′ CGG GTG GAA GGA AAT TTG TA 3′ Reverse 5′ TAG CAC TCA GGA GGG TGA GG 3′

4.7 | Scanning electron microscopy

E10.5 BAs and E12.5-E18.5 tongues from *Wnt1-Cre/caAlk2* mutants and *Cre⁻/caAlk2* littermate controls were fixed in 2.5% glutaraldehyde (#75520; Electron Microscopy Science, Hatfield, PA) and 4% PFA in 0.1 M PBS at room temperature for 24 hr. Tongues were then rinsed in 0.1 M PBS and subsequently postfixed in a sequence of aqueous 1% OsO_4 (#19150; Electron Microscopy Science, Hatfield, PA), 1% tannic acid (#16201; Sigma Aldrich, St. Louis, MO), 1% OsO_4, at 4°C for 1 hr each. Tissues were then dehydrated through an ascending series of ethanol (35, 50, 70, 90, and 100%, three changes at each concentration); and ethanol was displaced by three changes of hexamethyldisilazane (HMDS, #440191; Sigma Aldrich, St. Louis, MO) for 45 min each. Residual HMDS was evaporated slowly in a fume hood until the tissues were completely dry. Tissues were mounted onto specimen stubs, lightly sputter-coated with gold/palladium (Leica Gold/Carbon coater; Georgia Electron Microscope Core Facility, University of Georgia) and imaged using a scanning electron microscope (FEI Teneo FE-SEM; Georgia Electron Microscope Core Facility, University of Georgia).

4.8 | Photomicroscopy and data analyses

Immunostained whole mount tissues were imaged under a stereomicroscope (Olympus SZX16). Sections were examined thoroughly under a fluorescent light microscope (EVOS FL, Life Technologies). Colocalization of immunosignals was confirmed and photographed using a laser-scanning confocal microscope (Zeiss LSM 710, Biomedical Microscopy Core at the University of Georgia). Adobe Photoshop (2015) was used for figure assembling and image editing was minimal to improve clarity.

Quantitative analyses were made to obtain the number of p-Smad1/5/8⁺, cleaved (c) Caspase-3⁺, Ki67⁺, and DAPI⁺ total mesenchymal cells per unit area (mm²) on BA sections. Immunoreacted serial transverse sections of *Cre⁻/caAlk2* littermate control (n = 3) and *Wnt1-Cre/caAlk2* (n = 3) BAs were thoroughly examined under a fluorescent light microscope (EVOS FL, Life Technologies). Single-plane laser scanning confocal photomicrographs were obtained from every other sections to include the representative and corresponding

regions of BAs of littermate control and *Wnt1-Cre/caAlk2* mutants. Ki67$^+$ and DAPI$^+$ mesenchymal cells were counted in a selected area of BAs, while p-Smad1/5/8$^+$ and cCaspase-3$^+$ cells were quantified in the entire BAs 1–4 on every other sections.

Measurements of the length and width of the tongues were performed using the images of Shh immunostained E12.5 littermate control (*n* = 3) and *Wnt1-Cre/caAlk2* mutant (*n* = 3) tongues. The distance between the anterior most point and posterior end of Shh$^+$ circumvallate papilla placode was considered as the length. The widest region in the anterior 2/3 of the oral tongue was taken as the width. NIH-ImageJ software was used to measure the length and width of E12.5 tongues, western blot band intensities and the area of individual BAs. For the quantitative RT-PCR, changes of gene expression levels in individual BAs of *Wnt1-Cre/caAlk2* and littermate control groups were presented as means ± standard deviation (*X* ± *SD*; *n* = 3) of $2^{-\Delta CT}$ values.

Student's *t* test was used for the statistical analysis of the tongue length and width, and intensities of western blot bands of p-Smads between E12.5 *Wnt1-Cre/caAlk2* mutants and littermate controls. One-way analysis of variance (ANOVA) followed by Fisher's least significant difference (LSD) analyses was performed to test the statistical significance of gene expression levels among individual BAs of E10.5 *C57BL/6J* WT and *C57BL/6J WT/caAlk2* embryos. Two-way ANOVA followed by Fisher's LSD analyses was used to compare the gene expression levels in individual BAs between *Wnt1-Cre/caAlk2* and *Cre$^-$/caAlk2* littermate controls. A *p* value <.05 was taken as a statistically significant difference.

CONFLICT OF INTEREST

No conflict of interests declared.

ORCID

Yuji Mishina https://orcid.org/0000-0002-6268-4204
Hong-Xiang Liu https://orcid.org/0000-0001-5515-9869

REFERENCES

Beites, C. L., Hollenbeck, P. L. W., Kim, J., Lovell-Badge, R., Lander, A. D., & Calof, A. L. (2009). Follistatin modulates a BMP autoregulatory loop to control the size and patterning of sensory domains in the developing tongue. *Development*, 136(13), 2187–2197. https://doi.org/10.1242/dev.030544

Boggs, K., Venkatesan, N., Mederacke, I., Komatsu, Y., Stice, S., Schwabe, R. F., ... Liu, H. X. (2016). Contribution of underlying connective tissue cells to taste buds in mouse tongue and soft palate. *PLoS One*, 11(1), e0146475. https://doi.org/10.1371/journal.pone.0146475

Bragdon, B., Moseychuk, O., Saldanha, S., King, D., Julian, J., & Nohe, A. (2011). Bone morphogenetic proteins: A critical review. *Cellular Signalling*, 23(4), 609–620. https://doi.org/10.1016/j.cellsig.2010.10.003

Castillo, D., Seidel, K., Salcedo, E., Ahn, C., de Sauvage, F. J., Klein, O. D., & Barlow, L. A. (2014). Induction of ectopic taste buds by SHH reveals the competency and plasticity of adult lingual epithelium. *Development*, 141(15), 2993–3002. https://doi.org/10.1242/dev.107631

Chai, Y., & Maxson, R. E., Jr. (2006). Recent advances in craniofacial morphogenesis. *Developmental Dynamics*, 235(9), 2353–2375. https://doi.org/10.1002/dvdy.20833

Chandrashekar, L., Kashinath, K. R., & Suhas, S. (2014). Labial ankyloglossia associated with oligodontia: A case report. *Journal of Dentistry*, 11(4), 481–484.

Cobourne, M. T., Iseki, S., Birjandi, A. A., Adel Al-Lami, H., Thauvin-Robinet, C., Xavier, G. M., & Liu, K. J. (2018). How to make a tongue: Cellular and molecular regulation of muscle and connective tissue formation during mammalian tongue development. *Seminars in Cell & Developmental Biology*, 91, 45–54. https://doi.org/10.1016/j.semcdb.2018.04.016

Cordero, D. R., Brugmann, S., Chu, Y., Bajpai, R., Jame, M., & Helms, J. A. (2011). Cranial neural crest cells on the move: Their roles in craniofacial development. *American Journal of Medical Genetics. Part A*, 155A(2), 270–279. https://doi.org/10.1002/ajmg.a.33702

Farbman, A. I., & Mbiene, J.-P. (1991). Early development and innervation of taste bud-bearing papillae on the rat tongue. *Journal of Comparative Neurology*, 304(2), 172–186. https://doi.org/10.1002/cne.903040203

Fritzsch, B., Sarai, P. A., Barbacid, M., & Silos-Santiago, I. (1997). Mice with a targeted disruption of the neurotrophin receptor trkB lose their gustatory ganglion cells early but do develop taste buds. *International Journal of Developmental Neuroscience*, 15(4), 563–576. https://doi.org/10.1016/S0736-5748(96)00111-6

Fukuda, T., Scott, G., Komatsu, Y., Araya, R., Kawano, M., Ray, M. K., ... Mishina, Y. (2006). Generation of a mouse with conditionally activated signaling through the BMP receptor, ALK2. *Genesis*, 44(4), 159–167. https://doi.org/10.1002/dvg.20201

Grönroos, E., Kingston, I. J., Ramachandran, A., Randall, R. A., Vizán, P., & Hill, C. S. (2012). Transforming growth factor β inhibits bone morphogenetic protein-induced transcription through novel phosphorylated Smad1/5-Smad3 complexes. *Molecular and Cellular Biology*, 32(14), 2904–2916. https://doi.org/10.1128/MCB.00231-12

Ito, A., Nosrat, I. V., & Nosrat, C. A. (2010). Taste cell formation does not require gustatory and somatosensory innervation. *Neuroscience Letters*, 471(3), 189–194. https://doi.org/10.1016/j.neulet.2010.01.039

Iwata, J.-I., Suzuki, A., Pelikan, R. C., Ho, T.-V., & Chai, Y. (2013). Non-canonical transforming growth factor β (TGFβ) signaling in cranial neural crest cells causes tongue muscle developmental defects. *The Journal of Biological Chemistry*, 288(41), 29760–29770. https://doi.org/10.1074/jbc.M113.493551

Jung, H.-S., Oropeza, V., & Thesleff, I. (1999). Shh, Bmp-2, Bmp-4 and Fgf-8 are associated with initiation and patterning of mouse tongue papillae. *Mechanisms of Development*, 81(1), 179–182. https://doi.org/10.1016/S0925-4773(98)00234-2

Jussila, M., & Thesleff, I. (2012). Signaling networks regulating tooth organogenesis and regeneration, and the specification of dental mesenchymal and epithelial cell lineages. *Cold Spring Harbor Perspectives in Biology*, 4(4), a008425–a008425. https://doi.org/10.1101/cshperspect.a008425

Kawasaki, K., Porntaveetus, T., Oommen, S., Ghafoor, S., Kawasaki, M., Otsuka-Tanaka, Y., ... Ohazama, A. (2012). Bmp signalling in filiform tongue papillae development. *Archives of Oral Biology*, 57(6), 805–813. https://doi.org/10.1016/j.archoralbio.2011.11.014

Leikola, A. (1976). The neural crest: Migrating cells in embryonic development. *Folia Morphologica*, 24(2), 155–172.

Li, L., Wang, Y., Lin, M., Yuan, G., Yang, G., Zheng, Y., & Chen, Y. (2013). Augmented BMPRIA-mediated BMP signaling in cranial neural crest lineage leads to cleft palate formation and delayed tooth differentiation. *PLoS One*, *8*(6), e66107. https://doi.org/10.1371/journal.pone.0066107

Liu, H.-X., Grosse, A. M. S., Walton, K. D., Saims, D. A., Gumucio, D. L., & Mistretta, C. M. (2009). WNT5a in tongue and fungiform papilla development. *Annals of the New York Academy of Sciences*, *1170*, 11–17. https://doi.org/10.1111/j.1749-6632.2009.04369.x

Liu, H.-X., Grosse, A. S., Iwatsuki, K., Mishina, Y., Gumucio, D. L., & Mistretta, C. M. (2012). Separate and distinctive roles for Wnt5a in tongue, lingual tissue and taste papilla development. *Developmental Biology*, *361*(1), 39–56. https://doi.org/10.1016/j.ydbio.2011.10.009

Liu, H.-X., Henson, B. S., Zhou, Y., D'Silva, N. J., & Mistretta, C. M. (2008). Fungiform papilla pattern: EGF regulates inter-papilla lingual epithelium and decreases papilla number by means of PI3K/Akt, MEK/ERK, and p38 MAPK signaling. *Developmental dynamics*, *237*(9), 2378–2393. https://doi.org/10.1002/dvdy.21657

Liu, H. X., Komatsu, Y., Mishina, Y., & Mistretta, C. M. (2012). Neural crest contribution to lingual mesenchyme, epithelium and developing taste papillae and taste buds. *Developmental Biology*, *368*(2), 294–303. https://doi.org/10.1016/j.ydbio.2012.05.028

Liu, H.-X., MacCallum, D. K., Edwards, C., Gaffield, W., & Mistretta, C. M. (2004). Sonic hedgehog exerts distinct, stage-specific effects on tongue and taste papilla development. *Developmental Biology*, *276*(2), 280–300. https://doi.org/10.1016/j.ydbio.2004.07.042

Mayor, R., & Theveneau, E. (2013). The neural crest. *Development*, *140*(11), 2247–2251. https://doi.org/10.1242/dev.091751

Mbiene, J.-P., Maccallum, D. K., & Mistretta, C. M. (1997). Organ cultures of embryonic rat tongue support tongue and gustatory papilla morphogenesis in vitro without intact sensory ganglia. *Journal of Comparative Neurology*, *377*(3), 324–340. https://doi.org/10.1002/(SICI)1096-9861(19970120)377:3<324::AID-CNE2>3.0.CO;2-4

Merrill, A. E., Eames, B. F., Weston, S. J., Heath, T., & Schneider, R. A. (2008). Mesenchyme-dependent BMP signaling directs the timing of mandibular osteogenesis. *Development*, *135*(7), 1223–1234. https://doi.org/10.1242/dev.015933

Millington, G., Elliott, K. H., Chang, Y.-T., Chang, C.-F., Dlugosz, A., & Brugmann, S. A. (2017). Cilia-dependent GLI processing in neural crest cells is required for tongue development. *Developmental Biology*, *424*(2), 124–137. https://doi.org/10.1016/j.ydbio.2017.02.021

Mistretta, C. M. (1972). Topographical and histological study of the developing rat tongue, palate and taste buds. In J. F. Bosma (Ed.), *Oral sensation and perception: The mouth of the infant* (pp. 163–187). Springfield, IL: Thomas.

Mistretta, C. M., Liu, H.-X., Gaffield, W., & MacCallum, D. K. (2003). Cyclopamine and jervine in embryonic rat tongue cultures demonstrate a role for Shh signaling in taste papilla development and patterning: Fungiform papillae double in number and form in novel locations in dorsal lingual epithelium. *Developmental Biology*, *254*(1), 1–18. https://doi.org/10.1016/S0012-1606(02)00014-3

Parada, C., & Chai, Y. (2015). Mandible and tongue development. *Current Topics in Developmental Biology*, *115*, 31–58. https://doi.org/10.1016/bs.ctdb.2015.07.023

Parada, C., Han, D., & Chai, Y. (2012). Molecular and cellular regulatory mechanisms of tongue myogenesis. *Journal of Dental Research*, *91*(6), 528–535. https://doi.org/10.1177/0022034511434055

Pietsch, E. C., Sykes, S. M., McMahon, S. B., & Murphy, M. E. (2008). The p53 family and programmed cell death. *Oncogene*, *27*(50), 6507–6521. https://doi.org/10.1038/onc.2008.315

Puthiyaveetil, J. S. V., Kota, K., Chakkarayan, R., Chakkarayan, J., & Thodiyil, A. K. P. (2016). Epithelial—Mesenchymal interactions in tooth development and the significant role of growth factors and genes with emphasis on mesenchyme: A review. *Journal of Clinical and Diagnostic Research*, *10*(9), ZE05–ZE09. https://doi.org/10.7860/JCDR/2016/21719.8502

Ren, W., Aihara, E., Lei, W., Gheewala, N., Uchiyama, H., Margolskee, R. F., … Jiang, P. (2017). Transcriptome analyses of taste organoids reveal multiple pathways involved in taste cell generation. *Scientific Reports*, *7*(1), 4004. https://doi.org/10.1038/s41598-017-04099-5

Ribatti, D., & Santoiemma, M. (2014). Epithelial-mesenchymal interactions: A fundamental developmental biology mechanism. *The International Journal of Developmental Biology*, *58*(5), 303–306. https://doi.org/10.1387/ijdb.140143dr

Rinon, A., Lazar, S., Marshall, H., Büchmann-Møller, S., Neufeld, A., Elhanany-Tamir, H., … Tzahor, E. (2007). Cranial neural crest cells regulate head muscle patterning and differentiation during vertebrate embryogenesis. *Development*, *134*(17), 3065–3075. https://doi.org/10.1242/dev.002501

Serbedzija, G. N., Bronner-Fraser, M., & Fraser, S. E. (1992). Vital dye analysis of cranial neural crest cell migration in the mouse embryo. *Development*, *116*(2), 297–307.

Suga, T., Fukui, T., Shinohara, A., Luan, X., Diekwisch, T. G. H., Morito, M., & Yamane, A. (2007). BMP2, BMP4, and their receptors are expressed in the differentiating muscle tissues of mouse embryonic tongue. *Cell and Tissue Research*, *329*(1), 103–117. https://doi.org/10.1007/s00441-007-0416-4

Thesleff, I. (2003). Epithelial-mesenchymal signalling regulating tooth morphogenesis. *Journal of Cell Science*, *116*(9), 1647–1648. https://doi.org/10.1242/jcs.00410

Thirumangalathu, S., Harlow, D. E., Driskell, A. L., Krimm, R. F., & Barlow, L. A. (2009). Fate mapping of mammalian embryonic taste bud progenitors. *Development*, *136*(9), 1519–1528. https://doi.org/10.1242/dev.029090

Trainor, P. A. (2015). Preface. In P. A. Trainor (Ed.), *Current topics in developmental biology* (Vol. 111, pp. xv–xvi). Cambridge, MA: Academic Press.

Venkatesan, N., Boggs, K., & Liu, H.-X. (2016). Taste bud Labeling in whole tongue epithelial sheet in adult mice. *Tissue Engineering. Part C, Methods*, *22*(4), 332–337. https://doi.org/10.1089/ten.TEC.2015.0377

Wang, R. N., Green, J., Wang, Z., Deng, Y., Qiao, M., Peabody, M., … Shi, L. L. (2014). Bone morphogenetic protein (BMP) signaling in development and human diseases. *Genes & Diseases*, *1*(1), 87–105. https://doi.org/10.1016/j.gendis.2014.07.005

Yang, K., Hitomi, M., & Stacey, D. W. (2006). Variations in cyclin D1 levels through the cell cycle determine the proliferative fate of a cell. *Cell Division*, *1*, 32–32. https://doi.org/10.1186/1747-1028-1-32

Zhong, Z., Zhao, H., Mayo, J., & Chai, Y. (2015). Different requirements for Wnt signaling in tongue myogenic subpopulations. *Journal of Dental Research*, *94*(3), 421–429. https://doi.org/10.1177/0022034514566030

Zhou, Y., Liu, H.-X., & Mistretta, C. M. (2006). Bone morphogenetic proteins and noggin: Inhibiting and inducing fungiform taste papilla development. *Developmental Biology*, *297*(1), 198–213. https://doi.org/10.1016/j.ydbio.2006.05.022

Zhu, X.-J., Yuan, X., Wang, M., Fang, Y., Liu, Y., Zhang, X., … Zhang, Z. (2017). A Wnt/Notch/Pax7 signaling network supports tissue integrity in tongue development. *The Journal of Biological Chemistry*, *292*(22), 9409–9419. https://doi.org/10.1074/jbc.M117.789438